

# Muscovite dehydration melting in Si-rich metapelites: microstructural evidence from trondhjemitic migmatites, Roded, Southern Israel

Michael Anenburg · Yaron Katzir

Received: 14 August 2012 / Accepted: 15 April 2013 / Published online: 26 May 2013  
© Springer-Verlag Wien 2013

**Abstract** Making a distinction between partial melting and subsolidus segregation in amphibolite facies migmatites is difficult. The only significant melting reactions at low-pressures, either vapour saturated or muscovite dehydration melting, do not produce melanocratic peritectic phases. If protoliths are Si-rich and K-poor, then peritectic sillimanite and K-feldspar will form in scarce amounts, and may be lost by retrograde rehydration. The Roded migmatites of southern Israel (northernmost Arabian Nubian Shield) formed at  $P = 4.5 \pm 1$  kbar and  $T \leq 700$  °C and include Si-rich, K-poor paragneissic paleosome and trondhjemitic leucosomes. The lack of K-feldspar in leucosomes was taken as evidence for the non-anatectic origin of the Roded migmatites (Gutkin and Eyal, *Isr J Earth Sci* 47:117, 1998). It is shown here that although the Roded migmatites experienced significant post-peak deformation and recrystallization, microstructural evidence for partial melting is retained. Based on these microstructures, coupled with pseudosection modelling, indicators of anatexis in retrograded migmatites are established. Phase diagram modelling of neosomes shows the onset of muscovite dehydration melting at 4.5 kbar and 660 °C, forming peritectic sillimanite and K-feldspar. Adjacent non-melted paleosomes lack muscovite and would thus not melt by this reaction. Vapour saturation was not attained, as it would have formed cordierite that does

not exist. Furthermore, vapour saturation would not allow peritectic K-feldspar to form, however K-feldspar is ubiquitous in melanosomes. Direct petrographic evidence for anatexis is rare and includes euhedral plagioclase phenocrysts in leucosomes and quartz-filled embayments in corroded plagioclase at leucosome-melanosome interfaces. In deformed and recrystallized rocks muscovite dehydration melting is inferred by: (1) lenticular K-feldspar enclosed by biotite in melanosomes, (2) abundant myrmekite in leucosomes, (3) muscovite–quartz symplectites after sillimanite in melanosomes and associated with myrmekite in leucosomes. While peritectic K-feldspar formed in melanosomes by muscovite dehydration melting reaction, K-feldspar crystallizing from granitic melt in adjacent leucosome was myrmekitized. Excess potassium was used in rehydration of sillimanite to muscovite.

## Introduction

Migmatites are complex metamorphic rocks in which an intermediate coloured rock is segregated into a lighter part (leucosome) and a darker part (melanosome), both of which together forming the neosome. Any residual part of the rock that had not segregated is termed ‘paleosome’. The cause for the segregation is commonly believed to be partial melting (anatexis), but other mechanisms that do not require the existence of melt, generally termed ‘metamorphic differentiation’ or ‘subsidius segregation’, have been proposed (Sawyer 2008a). In high grade ( $> 700$  °C) metapelitic provinces that contain migmatites, distinction between the two processes is possible using textural, mineralogical and chemical indicators (Sawyer 2008a). An important criterion for anatexis is the existence of peritectic phases such as cordierite, garnet and amphibole that

---

Editorial handling: G. Hoinkes

---

M. Anenburg (✉) · Y. Katzir  
Geological and Environmental Sciences, Ben-Gurion  
University of the Negev, Beer Sheva, Israel  
e-mail: michaela@post.bgu.ac.il

Y. Katzir  
e-mail: ykatzir@bgu.ac.il

form due to melting reactions (Johannes and Gupta 1982; Sawyer 1999; Cesare et al. 2009; Ferrero et al. 2012). However, in migmatites metamorphosed at lower temperatures and pressures ( $\sim 650$  °C,  $< 10$  kbar), the only significant melt-producing reactions are either vapour saturated or muscovite dehydration melting forming sillimanite and K-feldspar as peritectic phases (Thompson 1982; Clemens and Vielzeuf 1987; Spear et al. 1999). Partial melting of K-poor ( $\leq 2.2$  wt %  $K_2O$ ) and Si-rich ( $\sim 70$  wt %  $SiO_2$ ) metapelites would produce even scarcer amounts of peritectic crystals, compared to rocks of average metapelite composition ( $\sim 3.5$  and  $60$  wt %, respectively, Mahar et al. 1997). A further complication in distinguishing anatexis arises from the chemical composition of the leucosomes. Most leucosomes in metapelitic migmatites are granitic, but trondhjemitic or tonalitic compositions (lacking K-feldspar) are known as well (Sawyer 2008a). The origin of K-poor leucosomes have been attributed to (1) anatexis and melt loss in an open system, (2) subsolidus segregation, (3) a combination of both, or (4) retainment of melt produced by vapour saturation (Amit and Eyal 1976; Sawyer 1987, 2008a; Whitney and Irving 1994; Spear et al. 1999; Garcia-Casco et al. 2001; Sadek 2003; Cruciani et al. 2008). Thus a definitive answer as to whether the generation of K-poor leucosomes involves melting is precluded. Finally, retrograde deformation and recrystallization may erase direct mineralogical and structural evidence for anatexis (Vernon 2011). As a result, distinction between subsolidus segregation and anatexis is difficult and may lead to erroneous tectonic conclusions because melt bearing rocks behave rheologically different compared to completely solid rocks (Solar 2008; Sawyer et al. 2011).

Many migmatites worldwide are part of larger metamorphic provinces in which it is possible to follow a field gradient and infer a variety of reactions that lead to anatexis. However, this is not always the case. The Roded migmatites of southern Israel are exposed in a small,  $\sim 1\text{km}^3$  window, removed from any context of a wide metamorphic area. The Roded migmatites formed at a non-favorable setting for attaining and retaining melting indicators. Protoliths are K-poor and Si-rich, peak metamorphic temperatures do not exceed  $700$  °C and post-peak deformation is significant. Consequently, their origin is disputed: Gutkin and Eyal (1998) claim that the migmatites formed by subsolidus segregation while Katz et al. (1998) suggest anatexis. The migmatites are stromatic metatexite layers hosted in a refractory quartz-dioritic gneiss host. The only mafic mineral in the studied migmatites is biotite, and the leucosomes do not contain any K-feldspar. The rocks are strongly deformed, but relicts of the original microstructures of migmatization can still be observed. The purpose of this study is to take a closer look at the peak conditions inferred by these two studies (Gutkin and Eyal 1998; Katz et al.

1998) using thermodynamic modelling coupled with careful petrographic examination in an attempt to better understand the migmatization process of the Roded migmatites.

Migmatite nomenclature is after Sawyer (2008b). Mineral abbreviations are after Kretz (1983).

## Geological setting

The northernmost Arabian-Nubian Shield (ANS) exposes continental crust that formed and evolved during the Neoproterozoic East African Orogenesis (Fig. 1a, Stern 1994). In southern Israel metamorphic rocks occur in two different rock associations, each exposed at a separate geographical location: (1) the Elat association and (2) the Roded association (Fig. 1b). Metamorphic rocks from the Elat association are usually considered to be a continuation of the Taba metamorphic complex (TMC, Fig. 1c) that has been extensively studied in the past several decades (Shimron 1972; Amit and Eyal 1976; Garfunkel 1980; Eyal and Amit 1984; Matthews et al. 1989; Cosca et al. 1999; Sadek Ghabrial 2003; Abu El-Enen et al. 2004; Eliwa et al. 2008; Morag et al. 2011). The Roded association, despite the close geographical proximity to the Elat association, records, however, different metamorphic and structural evolution (Garfunkel 1980; Katz et al. 1998; Cosca et al. 1999; Morag et al. 2011). The Roded metamorphic complex (RMC) is located in the heart of the Roded association (Fig. 1b). Two major studies of the RMC have been performed. The western part (Har Shelomo) was studied by Gutkin (1996) and Gutkin and Eyal (1998), and the eastern part (Har Yedidya) by Katz (1997) and Katz et al. (1998). The majority of the RMC is occupied by a quartz-dioritic orthogneiss, but amphibolites, schists and metamorphosed dykes also occur. Migmatites are exposed along a  $2.5$  km long and  $0.5$  km wide E–W trending zone in the northern edge of the RMC (the area between ‘S’ and ‘Y’ in Fig. 1b). The migmatites are of metatexite stromatic form (the neosome) hosted in metapelitic paragneiss (the paleosome).

The origin of the Roded migmatites is disputed. Katz et al. (1998) claim that temperatures were high enough to cross the vapour saturated melting curve and cause anatexis, but they do not provide adequate evidence. Gutkin and Eyal (1998), on the other hand, compared the Roded migmatites to the Magrish migmatites from the TMC and found both rock suites to be similar. They adduce lack of K-feldspar in leucosomes and homogeneous plagioclase composition for their conclusion, based on criteria given by Ashworth (1985). Since the Magrish migmatites have been shown to form by subsolidus segregation (Amit and Eyal 1976; Eyal and Amit 1984; Abu El-Enen et al. 2009, although a study by Sadek Ghabrial 2003 favours anatexis), it was concluded that the Roded migmatites formed in the same way.

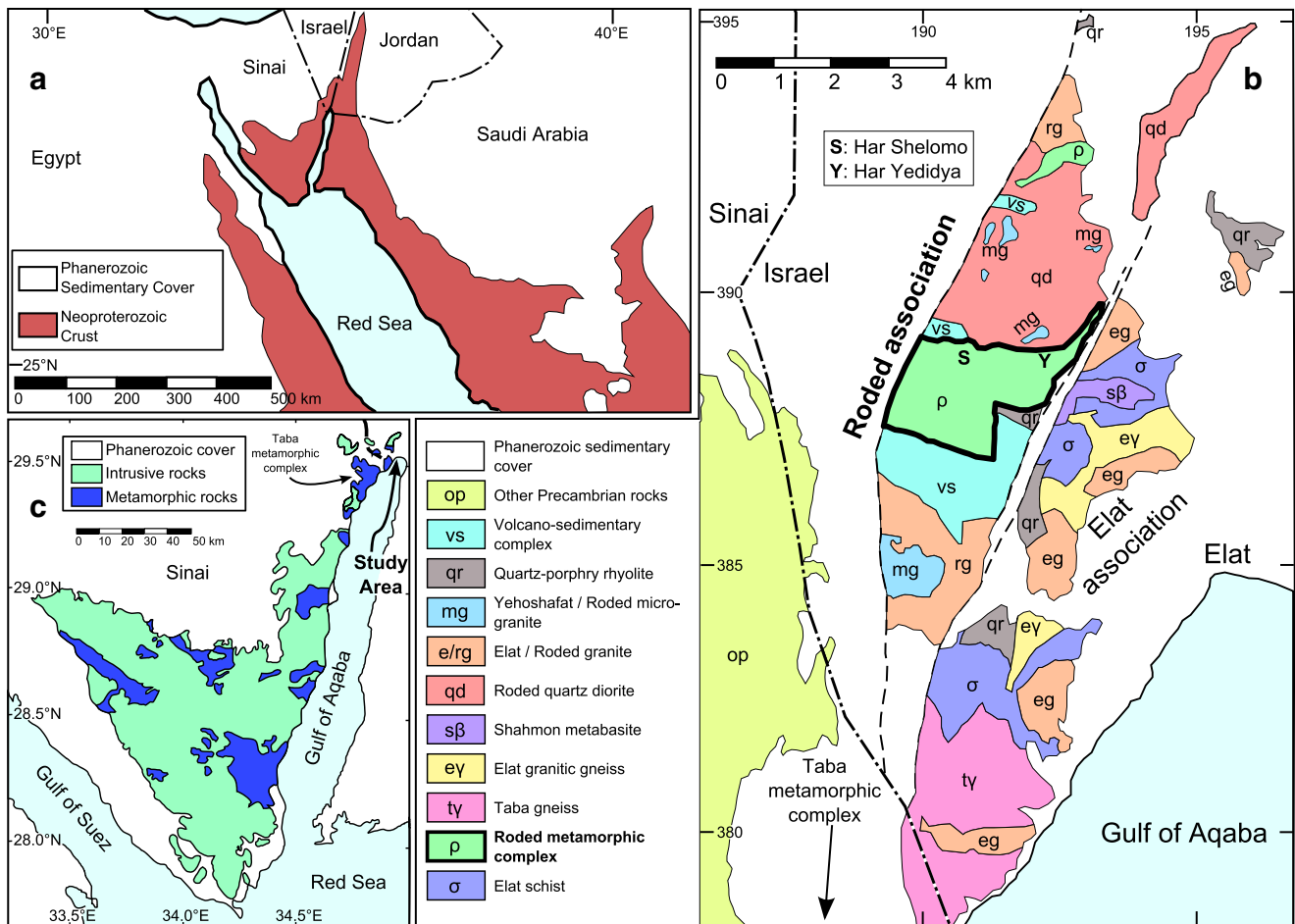


**Fig. 1** **a** Simplified geological map of the northern part of the ANS. **b** Simplified geological map of the ANS in southern Israel and Sinai (Egypt). **c** Geological map of the ANS in Israel. Study area is located in Har Shelomo (S) and Har Yedidya (Y). Coordinates are in the new

Israel grid. Bold outline marks the studied area of the RMC. Maps modified after Druckman et al. (1993), Abu-Alam and Stüwe (2009), and Morag et al. (2011)

Geothermobarometry of the migmatites by Gutkin and Eyal (1998) yielded peak temperatures ( $T$ ) of either 702 °C or 610 °C (using the models of Ferry and Spear 1978 and of Kleemann and Reinhardt 1994, respectively) at pressures ( $P$ ) of  $4.7 \pm 1$  kbar (using Ghent and Stout 1981). Katz et al. (1998) reported similar peak conditions of  $653 \pm 42$  °C (using Ferry and Spear 1978 and Holland and Blundy 1994) at a maximum  $P$  of 5 kbar (using Hollister et al. 1987) followed by retrograde metamorphism at  $558 \pm 44$  °C. It is not clear whether this retrograde equilibration represents a second metamorphic event or cooling of the first event (Katz et al. 1998). A fluid inclusion study by Gutkin et al. (1999) of the Roded migmatites constrained migmatization to occur between 610 °C at 2.5 kbar and 690 °C at 4.5 kbar based on the models of Kleemann and Reinhardt (1994) and Perchuk and Lavrent'eva (1983).

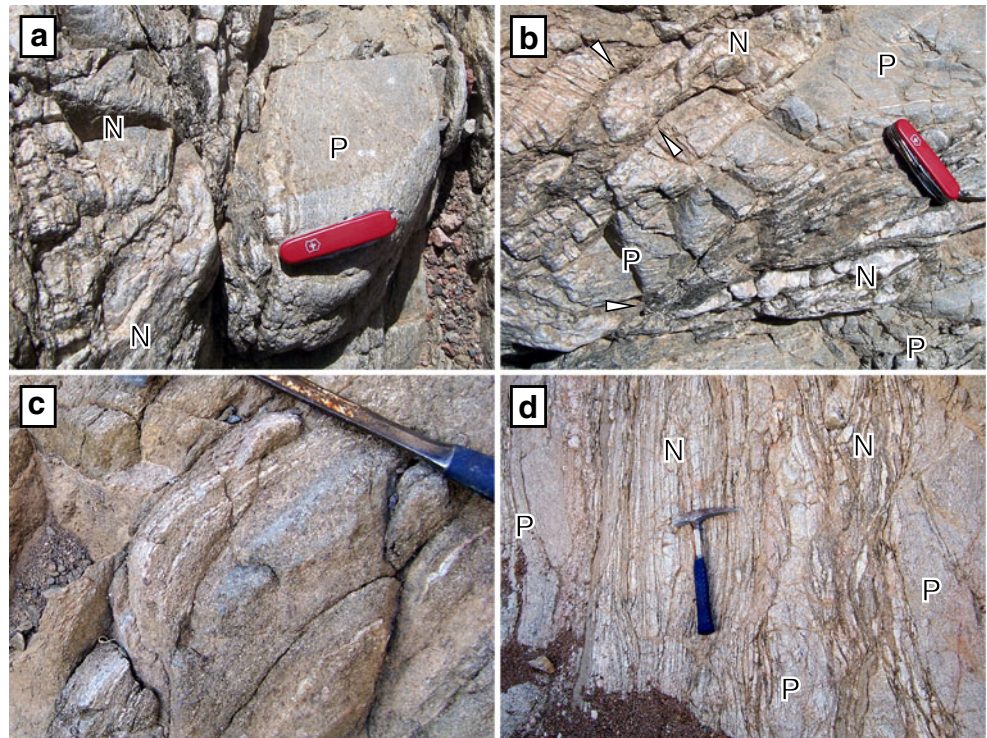
The timing of the metamorphic events in the RMC is poorly known. Katz et al. (1998) determined that

migmatization occurred prior to 725 Ma based on K–Ar dating. Morag et al. (2011) dated detrital zircons from the migmatites that record a magmatic age of ~800 Ma, and a poorly constrained lead loss event between 550 and 750 Ma.

### Field observations

The majority of Roded migmatite area is characterized by a weakly foliated paleosome (Fig. 2a, b). Neosomes are stromatic, several centimetres to several metres long, and show sub-parallel concordance to the paleosome foliation. The transition between paleosome and neosome is commonly sharp (Fig. 2d), but gradational transitions on the outcrop scale can also be seen (Fig. 2a). The gradational transition is characterized by an increasing abundance and size of neosomes as one progresses from the paleosome into the heart of the massive neosome.

**Fig. 2** **a** A photograph showing the gradational change from paleosome (P) in the centre to neosome (N) in the left. The phenocryst looking dots are in fact brown patina spots and are not part of the rock. **b** A photograph showing the fold structure associated with the rock in (a). Cuspate mica concentrations are shown with arrows. **c** A number of leucocratic veins located in a gneissose host. Note the absence of melanosome. **d** An outcrop exposed on the riverbed showing elongated neosomes



A closer look at the migmatites shows that they consist of concordant cm-wide stromatic metatexite neosomes with sharp contacts against the host paleosome (Fig. 3a). A less common second type of neosome is usually discordant with irregular contacts with the host rock foliation (Fig. 3b). A striking feature of the neosomes is that the grain size—in both leucosomes and melanosomes—is much coarser than the paleosome. Grain sizes in paleosomes are rarely larger

than 0.5 mm whereas some of the grains in the neosomes reach up to 2 mm.

The migmatites are deformed and folded (Fig. 2b), but undeformed neosomes also occur (Fig. 2d). When folding is intensive, thin cuspate shaped melanosomes are wedged between massive quartzo-feldspathic leucosome layers (Fig. 2b). The smaller leucosomes are not connected to any vein network, suggesting that they are *in situ* leucosomes.

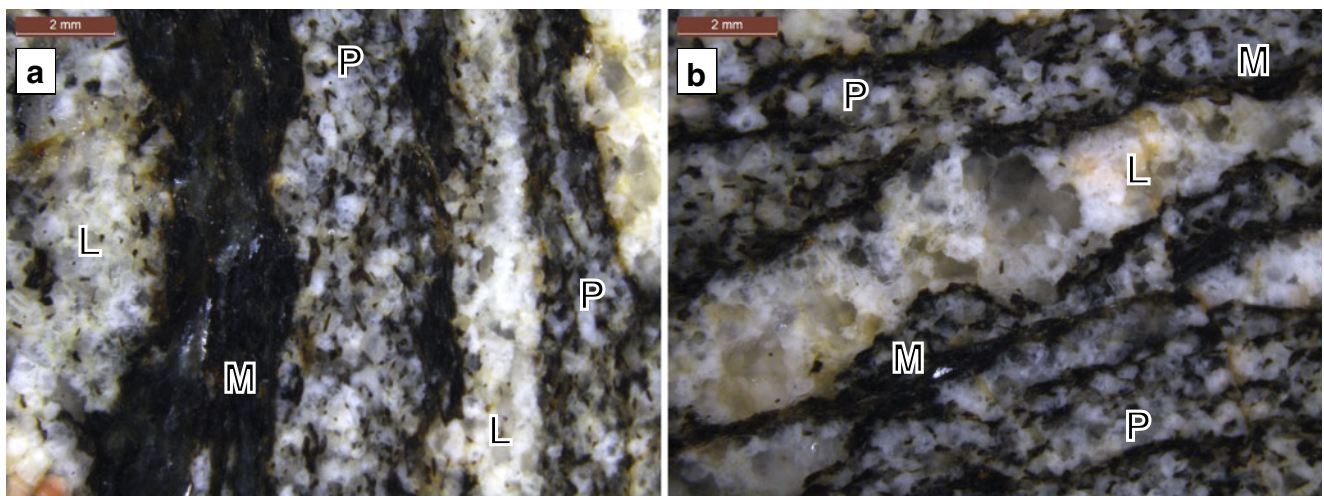


**Fig. 3** Two photographs of polished rock slabs showing: **a** Three different parts of the migmatite. The neosomes are mostly concordant to the paleosome foliation. **b** A patch of neosome that is discordant to the host paleosome. P: paleosome, L: leucosome, M: melanosome

However, isolated leucocratic veins without accompanying melanosomes can be found, suggesting an external source. They are usually concordant to the host rock foliation (Fig. 2c). Such leucocratic veins were described by Gutkin and Eyal (1998) and Gutkin et al. (1999) to be part of a later magmatic phase unrelated to the metamorphism.

### Petrography

In order to explore possible melting reactions in the Roded migmatites paleosomes and the most abundant, trondhjemitic, neosomes are studied. Although garnet, pinite pseudomorphs after cordierite and fibrolitic sillimanite have been reported to occur in the paleosome (Gutkin and Eyal 1998; Katz et al. 1998), here we will focus on rocks of a Si-rich composition that do not include these minerals. The reason for this is that the more mafic garnet and cordierite-bearing paleosomes are not related to the melting process, as these minerals occur only in paleosomes that do not exhibit migmatitic structures.

### Paleosome

The major mineral assemblage of the paleosomes is quartz+plagioclase+biotite±muscovite. A weak foliation is defined by biotite whereas muscovite is commonly discordant to it (Fig. 4a). In some cases muscovite encloses opaque mineral inclusions identified as ilmenite by Gutkin and Eyal (1998). Rare small K-feldspar grains occur either adjacent to biotite or enclosed by it.

### Neosome

The mineral assemblage of the leucosomes is dominated by quartz and plagioclase, some muscovite and negligible amounts of biotite. K-feldspar is not present in the leucosomes at all. We identify two types of leucosomes. In the first type, myrmekite (vermicular quartz in plagioclase, Fig. 4b) is very common and it is frequently in close association with muscovite (Fig. 4c, d). The myrmekite commonly shows somewhat oval quartz inclusions, but the entire shape spectrum spanning elongated to rounded inclusions

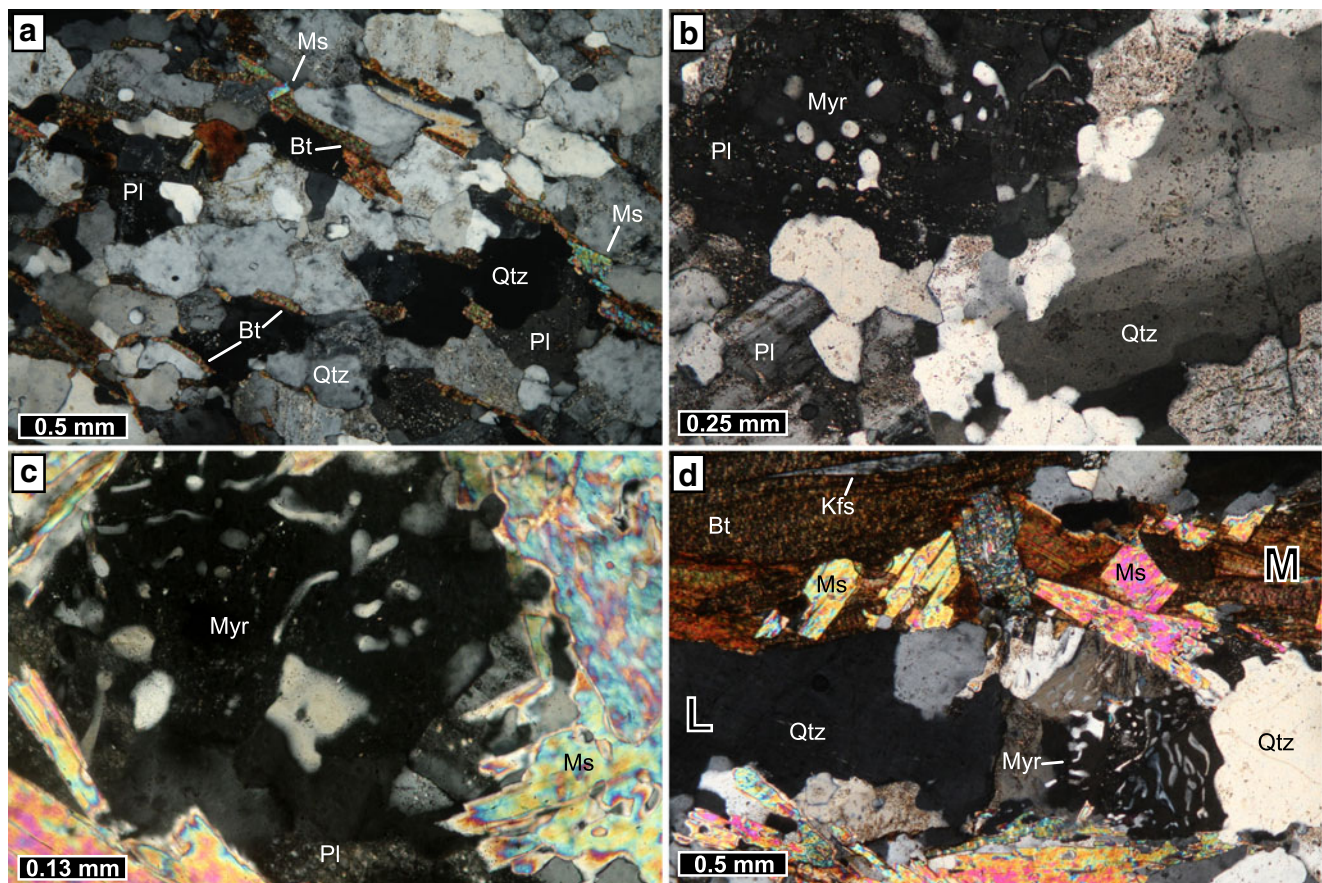


**Fig. 4** **a** The most common appearance of a paleosome. **b** Recrystallized myrmekite (Myr) in plagioclase, subgrain recrystallization in quartz and grain boundary migration. **c** Myrmekite and adjacent quartz-muscovite symplectites in a leucosome. **d** Myrmekite in

leucosome, quartz-muscovite symplectites in leucosome (bottom) and overprinting biotite in melanosome (top), elongated K-feldspar in melanosome

(Fig. 4b, c) is observed. Muscovite in the leucosomes contains symplectic quartz inclusions (Fig. 5a). Symplectites of muscovite and quartz frequently also overprint the adjacent melanosomes (Fig. 4d). One occurrence of a plagioclase phenocryst with well-developed crystal faces is observed in the leucosome. It occurs as an inclusion inside another plagioclase crystal (Fig. 5b). The second type of leucosome has some important differences compared to the first type: disrupted schollen consisting mostly of biotite, but also of muscovite and K-feldspar, exhibit the same morphology observed in the intact melanosomes described above (Fig. 5c). Schlieren showing imbrication of biotite crystals typical to diatexite migmatites suggest higher degree of melting (Fig. 5d, Sawyer 2008a, b). Myrmekite and quartz–muscovite symplectites are much less common in the second type than in the first type.

Melanosomes are composed of biotite, muscovite, K-feldspar and rarely plagioclase (Figs. 4d, 6a). Larger melanosomes also consist of muscovite rich cores surrounded by biotite rims (Fig. 6b). This muscovite only rarely shows quartz inclusions, but ilmenite inclusions are common. Lenticular and deformed K-feldspar is common

in melanosomes. It is almost always enclosed by biotite sheets and only rarely in contact with quartz or plagioclase (Figs. 4d, 5c, d, 6a, b, c). Zircon and monazite are common accessories in the melanosomes. The leucosome–melanosome interface is of great interest: embayments in corroded melanosome plagioclase grains are filled with one large quartz grain, which is part of the leucosome (Fig. 6c). Plagioclase in melanosomes never contains any myrmekite.

There are many signs of static recrystallization that post-dated deformation (Fig. 4b). Subgrain recrystallization is ubiquitous in large quartz leucosome grains. Grain boundary migration is also a common feature in both quartz and plagioclase grains.

### Pseudosections

Pseudosection modelling provides further insight on the melting reactions and assists in the interpretation of the microstructures. Here, we compare and model the bulk rock chemical analyses of two samples: MA-3 and MA-5 (Table 1a). These rocks are two representative samples from

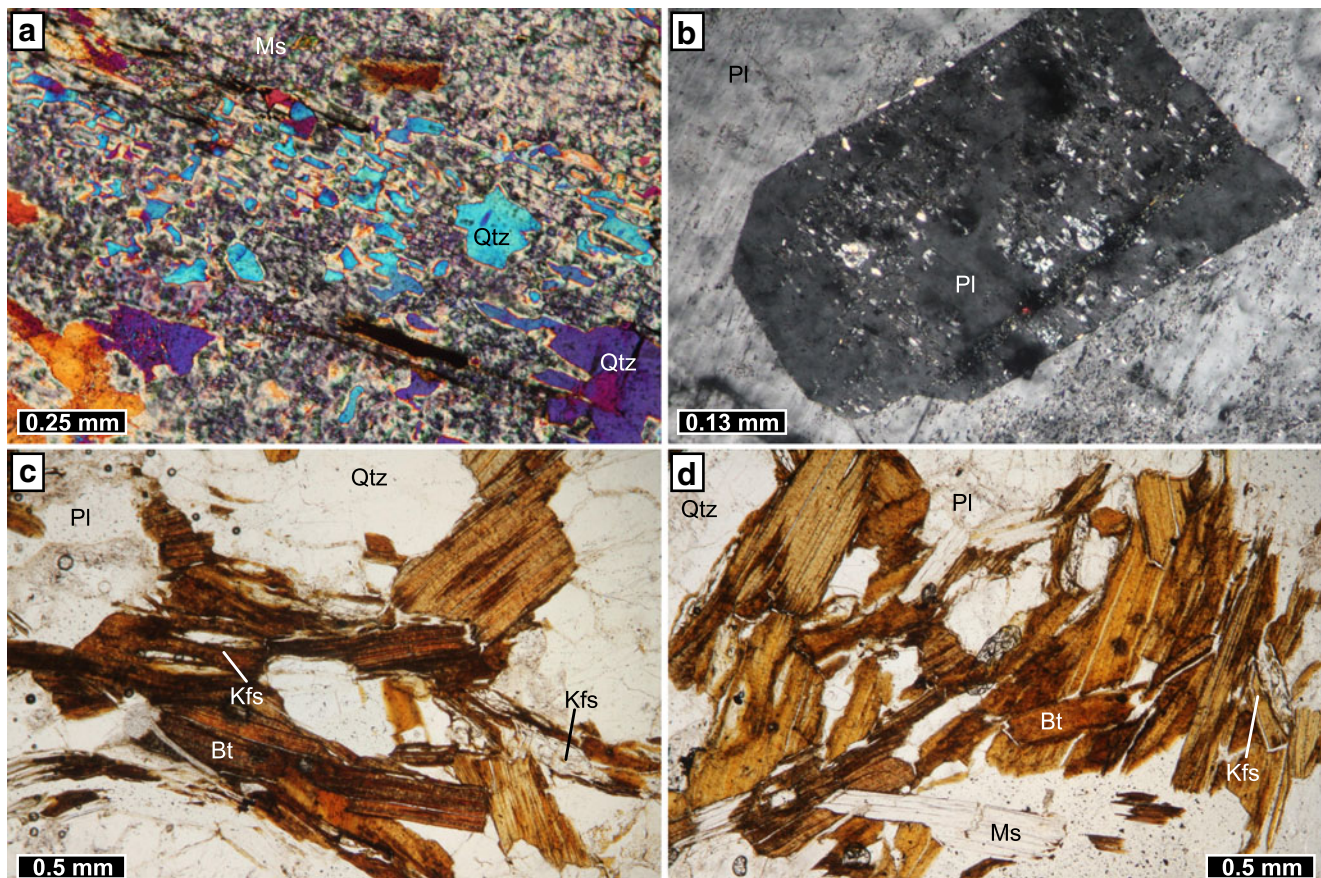


**Fig. 5** **a** Quartz–muscovite symplectites in a leucosome. **b** Plagioclase phenocryst in a leucosome. **c** A scholle of former melanosome inside a type two leucosome. **d** Schlieren showing imbricated biotite grains. Notice lack of quartz inclusions in muscovite

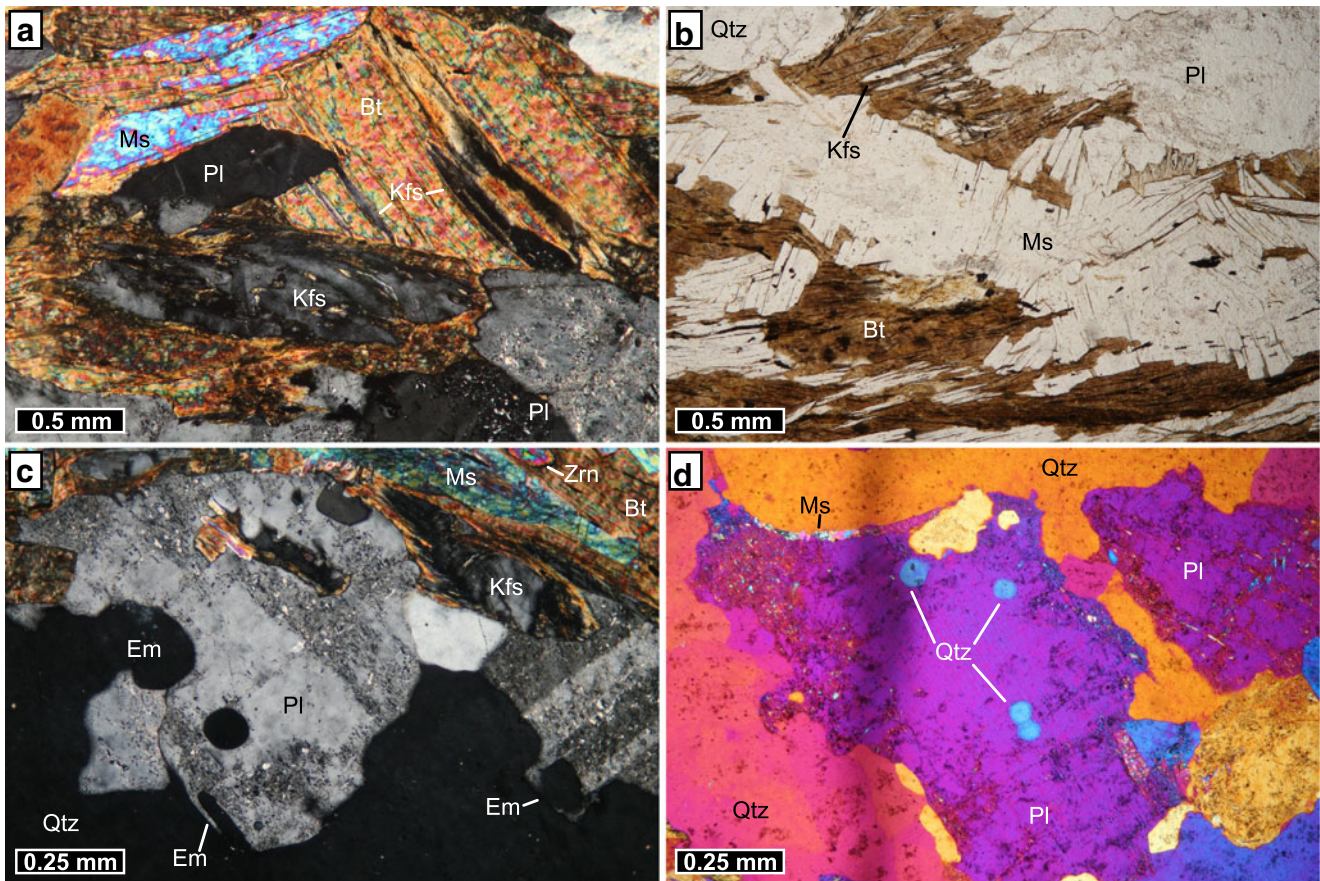


**Fig. 6** **a** Melanosome showing elongated plagioclase, K-feldspar oriented along biotite cleave planes, and discordant muscovite. **b** K-feldspar and discordant muscovite with abundant opaque inclusions in

melanosome. **c** Embayment (Em) in melanosome plagioclase grains at the interface with the leucosome (quartz). Notice K-feldspar grain. **d** Rounded quartz inclusions in plagioclase

**Table 1** Whole rock chemical compositions of a palaeosome (MA-3) and a neosome (MA-5) from Roded migmatites. a in wt %; b in mol %, used for phase diagram modelling

a	Bulk composition (wt %)		b	Modelling composition (mol %)	
	MA-3	MA-5		MA-3	MA-5
SiO <sub>2</sub>	71.26	70.03	SiO <sub>2</sub>	77.57	76.48
Al <sub>2</sub> O <sub>3</sub>	13.57	14.58	Al <sub>2</sub> O <sub>3</sub>	8.70	9.38
Fe <sub>2</sub> O <sub>3</sub> <sup>T</sup>	3.52	3.45	FeO	2.88	2.84
MnO	0.048	0.057	MgO	1.91	1.74
MgO	1.18	1.07	CaO	1.62	1.33
CaO	1.39	1.14	Na <sub>2</sub> O	4.04	3.84
Na <sub>2</sub> O	3.83	3.63	K <sub>2</sub> O	1.09	1.52
K <sub>2</sub> O	1.57	2.18	TiO <sub>2</sub>	0.42	0.37
TiO <sub>2</sub>	0.515	0.449	H <sub>2</sub> O	1.75	2.50
P <sub>2</sub> O <sub>5</sub>	0.08	0.11	Total	100.00	100.00
LOI	1.60	1.98			
Total	98.55	98.68			

a total of dozen analyses made for the Roded migmatites (unpublished data). Sample MA-3 consists of trondhjemitic palaeosome without any neosome patches and sample MA-5 is a pure neosome, including both melanosome and leucosome of the first type. The leucosome in sample MA-5 is an *in situ* leucosome so no melt loss has occurred and we consider the chemical composition of this sample to be similar to the original unmigmatized composition. This is also supported by the undepleted composition of MA-5 compared to MA-3: FeO and MgO contents are not higher in the neosomes than in the palaeosomes (Table 1a). Rock powders were analysed by ICP-OES in Activation Laboratories Ltd, Canada. MnO and P<sub>2</sub>O<sub>5</sub> were not used in modelling. FeO has been recalculated from Fe<sub>2</sub>O<sub>3</sub><sup>T</sup>. The amount of H<sub>2</sub>O used in the *P*–*T* diagrams is the minimum amount needed to initiate vapour saturated melting as determined using *T*–*X*(H<sub>2</sub>O) diagrams. Compositions for modelling are given in mol %, normalized to 100 % (Table 1b). The diagrams are calculated using *Perple\_X* (version 6.6.6, 18/12/2011 build, Connolly 2009). For a list of solution models used in the calculations of pseudosections in this paper, refer to Table 2. The

**Table 2** A summary of all solution models used in the construction of the sections

Symbol	Solution	Source
Bio(TCC)	Biotite	Tajčmanová et al. (2009)
feldspar	Feldspar	Fuhrman and Lindsley (1988)
Mica(CF)	Muscovite	Chatterjee and Froese (1975)
hCrld	cordierite	Holland and Powell (1998)
melt(HP)	NCKFMASH melt	Holland and Powell (2001); White et al. (2001)
Gt(HP)	Garnet	Holland and Powell (1998)
IlGkPy	Ilmenite	Ideal

pseudosections are calculated using the internally consistent thermodynamic database of Holland and Powell (1998, revised in 2002) in the NCKFMASHT ( $\text{Na}_2\text{O}-\text{CaO}-\text{K}_2\text{O}-\text{FeO}-\text{MgO}-\text{Al}_2\text{O}_3-\text{SiO}_2-\text{H}_2\text{O}-\text{TiO}_2$ ) system. The phase proportion diagram in Fig. 8c has been plotted using PyW-erami 2.0.1 by Ondrej Lexa using a Smooth factor of 1.0. Neosomes consisting of leucosomes of the second type are not modelled because of a sampling problem—the leucosome composition probably does not represent the initial melt, as will be shown later. Modelling of such a neosome would thus result in a meaningless mixture of melanosome and an unrelated leucosome. The isobaric  $T-X(\text{H}_2\text{O})$  diagrams are modelled with a pressure of 4.5 kbar, which is in agreement with most geobarometric estimates of the Roded migmatites (Gutkin and Eyal 1998; Katz et al. 1998; Gutkin et al. 1999).

Figure 7a shows a  $T-X(\text{H}_2\text{O})$  pseudosection for sample MA-3. According to the modelling, the rock can only melt by vapour saturated melting at  $\sim 670^\circ\text{C}$  given enough  $\text{H}_2\text{O}$  in the rock. Fig. 7b, modelled with 1.75 mol % of  $\text{H}_2\text{O}$  shows that this reaction is mostly independent of pressure. It is obvious that these conditions were not met as the rock shows no sign of melting. We are able to estimate the correct amount of  $\text{H}_2\text{O}$  present in the rock by the relative percentage of minerals. At 1.6 mol %  $\text{H}_2\text{O}$ , both cordierite and garnet are present in their minimum amounts (below 0.5 vol %). As no garnet or cordierite were found in the analysed rock 1.6 mol % seems like a reasonable estimate for the  $\text{H}_2\text{O}$  content of the rock.

Modelling of the neosome reveals a different picture. Pressure dependence is significant in MA-5, in contrast to MA-3 (Fig. 8a). However, different pressures only affect the temperatures in which reactions occur, and the topology of the reactions does not change in the range of  $P \simeq 4.5 \pm 1$  kbar. There are two main melting reactions portrayed in Fig. 8b. The first reaction, that occurs at  $\text{H}_2\text{O}$  contents higher than  $\sim 2.3$  mol %, is vapour saturated melting. This reaction can occur at lower temperatures in MA-5 than in MA-3 ( $645^\circ\text{C}$  and  $670^\circ\text{C}$ , respectively), suggesting a

more fertile composition for MA-5. At lower  $\text{H}_2\text{O}$  contents the melting temperature rises until it reaches  $660^\circ\text{C}$ . The second reaction, at  $\text{H}_2\text{O}$  contents of 1.7 to 2 mol %, is muscovite dehydration melting at  $660^\circ\text{C}$ . This reaction also occurs during vapour saturated melting, producing additional melt (Fig. 8c).

## Discussion

### Deformation and recrystallization

The migmatites were deformed in a ductile manner at post-peak metamorphic conditions: The cusped nature of the melanosomes (Fig. 2b) suggests that deformation occurred at a stage when melt had already crystallized and the leucosomes were competent layers, in contrast to the biotite rich melanosomes. Deformation of the rocks was followed by static recrystallization as evident by subgrain recrystallization and grain boundary migration. Both microstructures are formed at high temperatures and the rate is greatly increased by the presence of intergranular  $\text{H}_2\text{O}$  (Passchier and Trouw 2005; Vernon 2004). The presence of intergranular  $\text{H}_2\text{O}$  is evident by replacement of sillimanite by muscovite during retrograde processes, as will be discussed below. Due to post-peak deformation, not all microstructures seen today in the rocks are representative of the fabric present in the rock during migmatization. However, as strain is not uniformly distributed, some areas did not experience any significant post-peak deformation and likewise were not affected by retrograde recrystallization. As a result, there are rare textures that preserve direct evidence for anatexis. The euhedral shape of the plagioclase phenocryst observed in one of the leucosomes (Fig. 5b) requires the existence of melt (Vernon and Collins 1988; Vernon 2011). Additional evidence for anatexis are quartz-filled embayments in plagioclase crystals (Fig. 6c). This is the location of melt generation whereby plagioclase crystals are residual melanosome phases and the quartz crystal crystallized from an anatectic melt forming the leucosome. The quartz crystal is undeformed while most large quartz crystals in other parts of the rock show subgrain recrystallization. This suggests that this part of the rock was not strained and it escaped recrystallization, thus the adjacent embayments were not affected by static recrystallization as well.

Myrmekite is commonly affected by static recrystallization. Elongated quartz vermicules are rare and a more rounded shape is common (Fig. 4b). This can be explained by the tendency of static recrystallization to minimize the surface energy of grains and transform the elongated quartz into spherical quartz through the process of grain boundary area reduction (GBAR; Passchier and Trouw 2005). It is thus suggested that most, if not all, rounded quartz

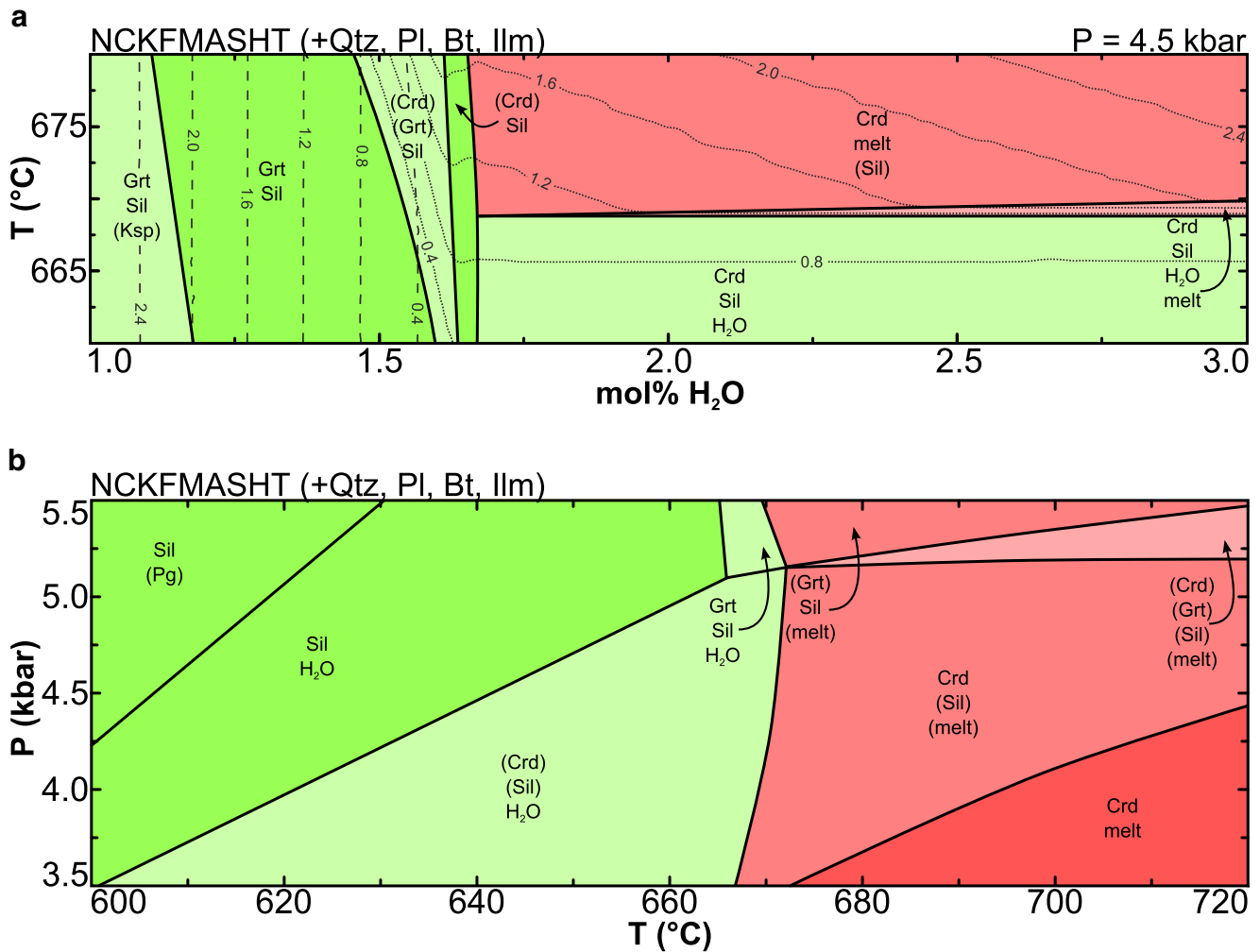
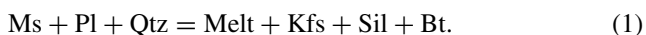


**Fig. 7** Pseudosections for sample MA-3. Negligible phases (less than 1 vol%) are in parentheses. Melt-bearing fields are red, melt absent fields are green. **a**  $T$ - $X(\text{H}_2\text{O})$  pseudosection. Dotted lines are vol % of cordierite. Dashed lines are vol % of garnet. **b**  $P$ - $T$  pseudosection

inclusions (e.g. Fig. 6d) are the result of recrystallized myrmekite.

#### Reaction microstructures

The muscovite dehydration melting reaction according to Patiño Douce and Harris (1998) is



This reaction is in agreement with the modelled phase relations from this study (Fig. 8). Generally, in migmatites, the peritectic K-feldspar, sillimanite and biotite should concentrate in the melanosomes. K-feldspar and sillimanite usually overgrow muscovite and the neo-formed biotite causes coarsening of pre-existing grains (Brown 2002). Melt produced by this reaction plots in the granite field of Barker's classification diagram (1979), including

plagioclase and K-feldspar ('granite minimum' composition, e.g. Johannes 1985). In the Roded migmatites, K-feldspar is observed in the melanosomes and biotite is coarser than in paleosomes, but no sillimanite occurs and the leucosomes do not contain K-feldspar. These discrepancies are explained by retrograde reactions that occurred during melt crystallization and formed myrmekite and quartz-muscovite symplectites on the expense of K-feldspar and sillimanite, respectively. Patiño Douce and Harris (1998) also consider an  $\text{H}_2\text{O}$  vapour saturated melting reaction:



This reaction produces trondhjemitic melts, but does not form K-feldspar as a peritectic mineral. However, all melanosomes in the Roded migmatites contain abundant K-feldspar. Although it is possible that a vapour saturated reaction occurred, an examination of the amounts of melt generated by each reaction in the contours of

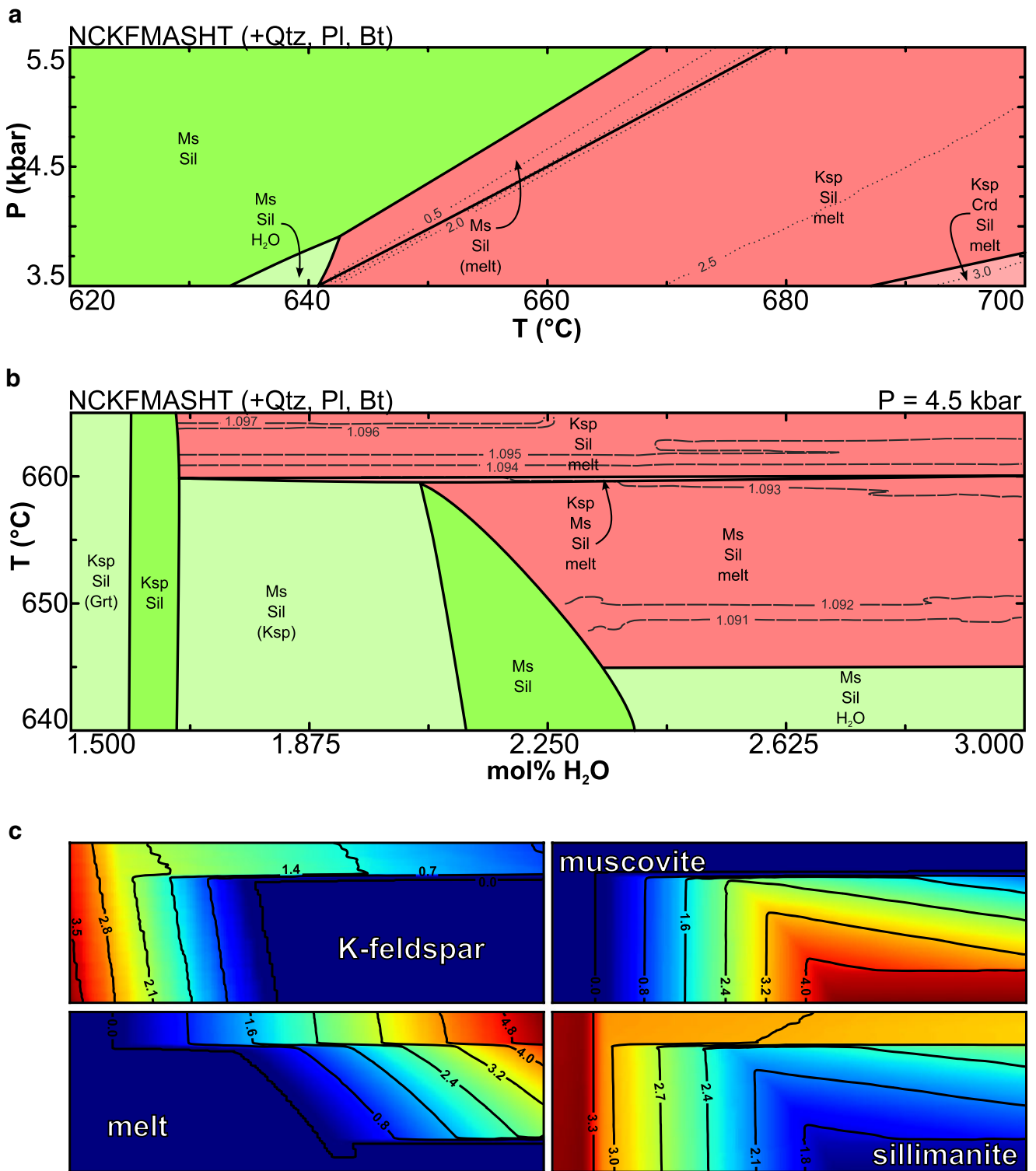


**Fig. 8** Pseudosections for sample MA-5. Negligible phases (less than 1 vol %) are in parentheses. Melt-bearing fields are red, melt absent fields are green. **a**  $P$ - $T$  pseudosection. Dotted lines are the vol % of

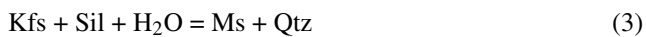
melt. **b**  $T$ - $X(\text{H}_2\text{O})$  pseudosection. Dashed lines are the  $A/\text{CNK}$  ratio of the melt. **c** Phase proportion diagrams for selected phases. Axes are identical to **b**. Values are in vol %

Fig. 8a shows that most melt is generated by muscovite dehydration. Higher degrees of melting by vapour saturation

would require larger amounts of  $\text{H}_2\text{O}$  (e.g. right side of the ‘melt’ diagram in Fig. 8c), but there is no evidence in the

rocks for any significant ingress of H<sub>2</sub>O. Evidently, the only melting reaction that occurred is muscovite dehydration without vapour saturation.

Myrmekite is commonly considered as a replacement of K-feldspar by plagioclase and quartz overgrowth (see Vernon 2004 for a review and Yuguchi and Nishiyama 2008 for a modern approach). The replacement of K-feldspar by myrmekite in migmatites is not uncommon and has been previously described (e.g. White 1966; Gupta and Johannes 1982; Ragab and El-Gharabawi 1989; Väisänen and Hölttä 1999; Harris et al. 2004; Hasalova et al. 2008), although in most cases the K-feldspar was not completely consumed. We suggest that in the Roded migmatites the leucosome K-feldspar was completely replaced. Although the amount of K-feldspar in the leucosomes cannot be measured quantitatively, a rough estimate of the ratios of myrmekite-free versus myrmekite-bearing plagioclase suggests that the melt composition was close to the 'granite minimum' composition of muscovite dehydration melting as shown in Patiño Douce and Harris (1998). A common feature of myrmekites in the Roded migmatites is the abundance of nearby quartz–muscovite symplectites (Fig. 4a, b). Wherever there is myrmekite, late non-preferentially oriented symplectic muscovite appears. Quartz–muscovite intergrowths have been previously described in association with sillimanite (e.g. Pognante 1992; Petřík and Janák 2002). The reaction commonly responsible for such microstructures is



as described in Brown (2002). The  $\frac{\text{Al}_2\text{O}_3}{2\text{CaO} + \text{Na}_2\text{O} + \text{K}_2\text{O}}$  ratio (A/CNK) of the melt is contoured in Fig. 8. Vapour saturation forms peraluminous melts with A/CNK  $\simeq$  1.092 but at higher temperatures, once muscovite dehydration takes action, this ratio is higher at A/CNK  $\geq$  1.095 which is close to the 'strong peraluminous' melts of the experiments conducted by Patiño Douce and Harris (1998). We argue that during melt crystallization excess K<sup>+</sup> cations released by myrmekitization were consumed in the hydration of peritectic sillimanite to form muscovite in the melanosomes, with additional K<sup>+</sup> cations forming muscovite adjacent to myrmekite in the leucosomes due to the peraluminous composition of the anatectic melt.

A recent study by Peterman and Grove (2010) has shown that quartz–muscovite symplectites can form at temperatures much lower (as much as 250 °C) than peak metamorphic temperatures. Furthermore, Vernon (2011) mentioned myrmekite as an unreliable evidence for the existence of partial melt, but rather a later metasomatic process. This is probably not the case here, since this does not explain why the deformed melanosome K-feldspar was not replaced and the leucosome K-feldspar was

completely replaced. The process suggested by Yuguchi and Nishiyama (2008) for the formation of myrmekite requires that K-feldspar would be in contact with plagioclase and that myrmekite forms in the final deuteric stage of magma crystallization. It is safe to assume that all of the K-feldspar crystallizing in leucosomes has been in contact with plagioclase. However, K-feldspar in melanosomes is usually not in contact with plagioclase so it should not be replaced, except of rare cases of melanosome K-feldspar in direct contact with plagioclase (e.g. Fig. 6a, c). According to the subsolidus model (Peterman and Grove 2010; Vernon 2011) this K-feldspar should have also been replaced by myrmekite. These K-feldspar grains are still present in the rock, supporting the deuteric model of Yuguchi and Nishiyama (2008). Thus, myrmekitization probably occurred at the last stages of melt crystallization (as suggested by Kohn et al. 1997, Spear et al. 1999 and Hasalová et al. 2008).

In three out of five analyses by electron microprobe (unpublished data), we detected  $1.11 \pm 0.15$  wt % of BaO in K-feldspars from the Roded migmatites. Nabelek and Bartlett (1998), in a study of migmatites and leucogranites, have shown that K-feldspar produced by muscovite dehydration melting should be enriched in barium, providing further support for the anatectic origin of the Roded migmatites. Curiously, barium-bearing K-feldspars intercalated with biotite sheets from non anatectic metapelitic schists have been described in the TMC by Abu El-Enen et al. (2004), but their occurrence is only mentioned in brief and we are unable to make a comparison.

#### Extent of migmatization

The crystallizing melt in the reactions described so far was assumed to be *in situ* initial melt not affected by differentiation or extraction processes. This is supported by the outcrop scale morphology of the migmatites. However, textural evidence for the occurrence of evolved melt in the leucosomes is seen in some places. A sample containing type two leucosomes was taken from a continuous wide neosome (Fig. 2a). This sample is characterized by diatexitic microstructures suggesting higher degree of melting compared to type one leucosomes. The melanosomes contain abundant K-feldspar formed by muscovite dehydration (Reaction 1), but myrmekite and quartz–muscovite symplectites are rare. This suggests that Reaction 3 seldom occurred and K-feldspar should have been retained in the leucosomes, but no K-feldspar is present. The initial K-rich melt was probably extracted, leaving a residual melt of trondhjemitic composition (e.g. Sawyer 2008a and sources therein). A second possibility is that the composition of these type two leucosomes represents cumulates, similar to the migmatites studied

by Solar and Brown (2001). Melt flow is indicated by abundant biotite schollen and biotite imbrication in schlieren in leucosomes (Fig. 5c, d). Such features require the existence of more melt implying more muscovite available for dehydration.

Rare lenticular K-feldspar also occurs in some paleosomes, suggesting muscovite dehydration. The minute amounts of K-feldspar suggest that any melt produced existed in vanishingly small amounts, and any retrograde deformation and recrystallization completely erased evidence for its former presence. This melting was caused by small amounts of muscovite present in these paleosomes at pre-anatexis conditions.

It is evident then, that the degree of melting in the Roded migmatites is controlled mainly by the amount of muscovite present in the rocks, which is in turn controlled by the chemical composition of the rocks. The chemical composition of the pre-anatexis rocks reflects the composition of the original sediment. A comparison of the analyses (Table 1) shows that while their compositions are overall similar, the neosome (MA-5) is slightly more pelitic, i.e. it has more  $K_2O$  and  $Al_2O_3$ . This slight variation was enough to stabilize muscovite in addition to biotite, which then facilitated muscovite dehydration melting.

The subsolidus migmatization mechanism offered by Eyal and Amit (1984) and Gutkin and Eyal (1998) does not explain the occurrence of K-feldspar in melanosomes and the muscovite microstructures. The almost exclusive association of such features with neosomes provides strong evidence for their genesis by anatexis. If the migmatites had formed by subsolidus segregation, leucosomes should also have appeared in parts of the rock with a more refractory composition, but this is not the case.

#### Late muscovite

So far, quartz–muscovite symplectites have been accounted for by Reaction 3, yet there are occurrences of muscovite without quartz inclusions in both neosomes and paleosomes (Figs. 4a, d, 5d, and 6a, c). Furthermore, sillimanite is predicted to occur in the rocks even in subsolidus conditions (Figs. 7, 8). Late post-kinematic muscovite is common in rocks from the Elat association (Shimron 1972) and elsewhere in the northern ANS (e.g. Kabesh et al. 2012), where it occasionally contains ilmenite inclusions, similar to such muscovites from the Roded migmatites (Fig. 6b).

This suggests replacement of sillimanite by muscovite during retrograde hydration of the rocks. Figure 9 shows modelled proportions of phases participating in the process for bulk composition MA-5. The modelled process is a linear retrograde path, starting at  $T = 630\text{ }^\circ\text{C}$ ;  $P = 4.5$  kbar;  $X(H_2O)=2.0$  mol % and ending at  $T = 530\text{ }^\circ\text{C}$ ;

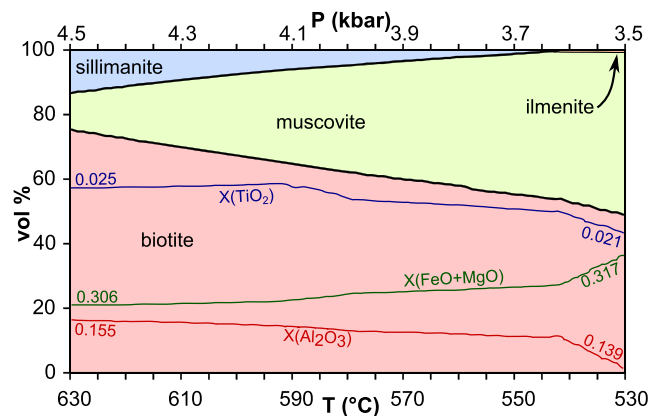
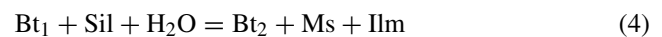


**Fig. 9** Relative vol % of selected phases in a retrograde path, starting with 2 mol % and ending with 3.5 mol % of  $H_2O$ . Coloured lines inside the biotite field show the variation of  $TiO_2$  (blue),  $FeO+MgO$  (green) and  $Al_2O_3$  (red) as retrogradation progresses. Axes are arbitrary, initial and final values are given at the left and right ends, respectively

$P = 3.5$  kbar;  $X(H_2O)=3.5$  mol %. The continuous reaction can be summarized as



where biotite<sub>2</sub> is less abundant than biotite<sub>1</sub> and contains higher contents of Mg and Fe and lower contents of Al and Ti (coloured lines in Fig. 9). Muscovite crystallizes at the expense of biotite and sillimanite, and the additional Ti precipitates as ilmenite. The remaining Mg and Fe are enriched in the resulting, less abundant, biotite. This reaction accounts for the ilmenite inclusions in muscovite observed in the rocks (Fig. 5a).

#### Model of migmatization in the RMC

A summary of our model for the formation of the Roded migmatites is shown in Fig. 10. The initial, pre-migmatized state of the rocks consisted of metapelites of variable composition (Fig. 10a), reflecting the chemical composition of the original pelitic sediment. It had layers rich in cordierite (not shown) and garnet, layers rich in biotite and layers rich in muscovite. Upon reaching peak  $T$ , muscovite dehydrated into sillimanite and K-feldspar, forming melt patches, the size of which is a function of the amount of muscovite available for dehydration (Fig. 10b). Once the melt crystallized, the rock contained trondhjemitic leucosomes with myrmekite after magmatic K-feldspar and quartz–muscovite symplectites after peritectic sillimanite (quartz not shown for simplicity), as portrayed in Fig. 10c. The final stage (Fig. 10d) involved replacement of the original sillimanite by discordant muscovite (ilmenite not shown for simplicity) and recrystallization of elongated myrmekite to rounded quartz inclusions. This is how fresh samples from the Roded migmatites look today.

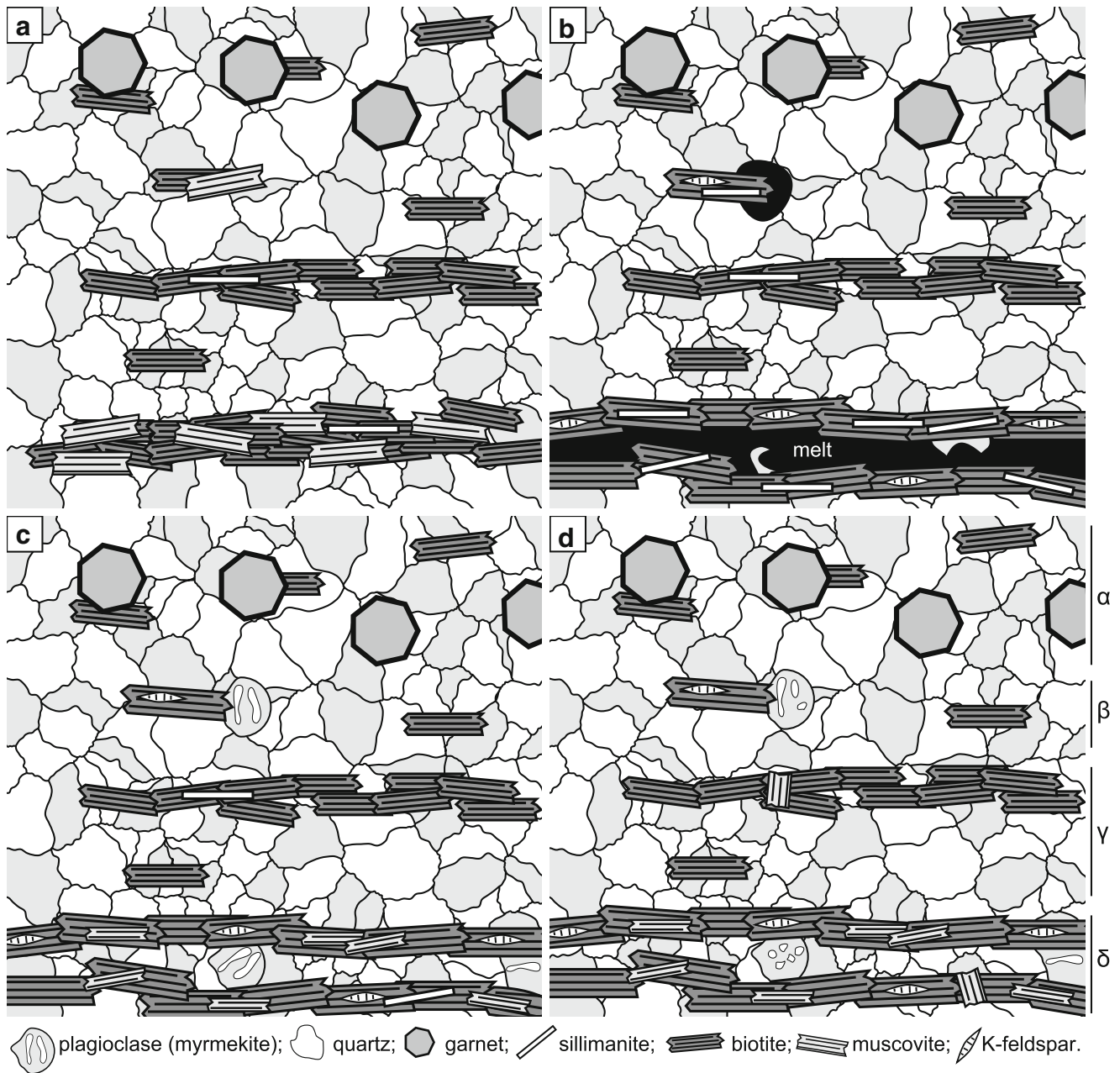


**Fig. 10** A not-to-scale cartoon showing the migmatization process in chronological order. The part of the rock marked by  $\alpha$  marks the cordierite and garnet bearing paleosome described in detail by previous studies (Gutkin and Eyal 1998; Katz et al. 1998; Gutkin et al. 1999).  $\beta$

marks the occasional isolated neosome observed in some paleosomes (e.g. Fig. 3b).  $\gamma$  and  $\delta$  mark the trondhjemitic paleosome and neosome used in modelling (MA-3 and MA-5, respectively)

## Conclusions

We have shown both direct and indirect evidence for anatexis in the Roded migmatites. Direct evidence includes embayments (Fig. 6c) and plagioclase phenocrysts (Fig. 5b). This evidence alone is sufficient to determine anatexis in migmatites (Holness et al. 2011). However, the Roded migmatites—and other migmatites worldwide—commonly experience retrograde recrystallization that erases such

direct evidence. In the case of muscovite dehydration melting, we show three criteria for inferring anatexis in recrystallized rocks:

1. Symplectic muscovite and quartz in melanosomes outgrowing peritectic sillimanite, possibly completely (Fig. 4d). This muscovite should not be confused with late retrograde muscovite that also outgrows sillimanite, but commonly includes ilmenite (Fig. 6b).

2. Symplectic muscovite and quartz associated with (commonly round due to recrystallization) myrmekite in leucosomes, suggesting replacement of K-feldspar crystallizing from granite-minimum melt (Figs. 4c, d, 5a).
3. Lenticular K-feldspar wedged between biotite sheets in melanosome (Figs. 4d, 5c, 6a, b).

Taken together, these three criteria may help distinguish anatexis from metamorphic differentiation in rocks that experienced retrograde deformation and recrystallization and direct evidence for melting (such as phenocrysts and embayments) no longer exists. In the case of migmatites of limited chemical composition such as the Roded migmatites (Si-rich and K-poor), these microstructures may be the only textural evidence for anatexis as other peritectic minerals did not form. Criteria 1 and 2 may be less common in cases of melt extraction as a result of higher degree of melting. As vapour saturated conditions were not attained, the degree of melting is controlled by the amount of muscovite (and thus, the amount of H<sub>2</sub>O) available in the rock prior to the onset of migmatization. In the T < 700 °C conditions hitherto discussed, temperature plays a minor role in the amount of melt generated.

**Acknowledgments** We wish to thank Omar Bartoli and an anonymous reviewer for constructive and thorough reviews. Discussions with Jamie Connolly concerning *Perple\_X* modelling are greatly appreciated. Emilie Bruand and Bernardo Cesare are thanked for their reviews of a previous version of the manuscript.

## References

- Abu-Alam TS, Stüwe K (2009) Exhumation during oblique transpression: The Feiran–Solaf region, Egypt. *J Metamorph Geol* 27:439–459. doi:10.1111/j.1525-1314.2009.00827.x
- Abu El-Enen MM, Will TM, Okrusch M (2004) *P–T* evolution of the Pan-African Taba metamorphic belt, Sinai, Egypt: Constraints from metapelitic mineral assemblages. *J Afr Earth Sci* 38:59–78. doi:10.1016/j.jafrearsci.2003.09.002
- Abu El-Enen MM, Zalata AA, El-Shakour ZAA (2009) Subsolidus and anatectic migmatites: Examples from the Pan-African crystalline basement, southern Sinai, Egypt. *Egypt J Geol* 53:63–86
- Amit O, Eyal Y (1976) The genesis of Wadi Magrish migmatites (N-E Sinai). *Contrib Mineral Petrol* 59:95–110. doi:10.1007/BF00375111
- Ashworth JR (1985) *Migmatites*. Blackie & Son, Glasgow
- Barker F (1979) Trondhjemitic: definition, environment and hypotheses of origin. In: Barker F (ed) *Trondhjemitic, Dacites and related Rocks*. *Developments in Petrology*, vol 6. Elsevier, Amsterdam
- Brown M (2002) Retrograde processes in migmatites and granulites revisited. *J Metamorph Geol* 20:25–40. doi:10.1046/j.0263-4929.2001.00362.x
- Cesare B, Ferrero S, Salvioli-Mariani E, Pedron D, Cavallo A (2009) “Nanogranite” and glassy inclusions: The anatectic melt in migmatites and granulites. *Geology* 37:627–630. doi:10.1130/G25759A.1
- Chatterjee ND, Froese E (1975) A thermodynamic study of the pseudobinary join muscovite–paragonite in the system KAlSi<sub>3</sub>O<sub>8</sub>–NaAlSi<sub>3</sub>O<sub>8</sub>–Al<sub>2</sub>O<sub>3</sub>–SiO<sub>2</sub>–H<sub>2</sub>O. *Am Mineral* 60:985–993
- Clemens JD, Vielzeuf D (1987) Constraints on melting and magma production in the crust. *Earth Planet Sc Lett* 86:287–306. doi:10.1016/0012-821X(87)90227-5
- Connolly JAD (2009) The geodynamic equation of state: What and how. *Geochem Geophys Geosyst* 10:Q10014. doi:10.1029/2009GC002540
- Cosca MA, Shimron A, Caby R (1999) Late Precambrian metamorphism and cooling in the Arabian–Nubian Shield: Petrology and <sup>40</sup>Ar/<sup>39</sup>Ar geochronology of metamorphic rocks of the Elat area (Southern Israel). *Precambrian Res* 98:107–127. doi:10.1016/S0301-9268(99)00044-3
- Cruciani G, Franceschelli M, Elter FM, Puxeddu M, Utzeri D (2008) Petrogenesis of Al–silicate-bearing trondhjemitic migmatites from NE Sardinia, Italy. *Lithos* 102:554–574. doi:10.1016/j.lithos.2007.07.023
- Druckman Y, Weissbrod T, Garfunkel Z (1993) Sheets 25, 26: Yotvata and Elat. Geological Map of Israel 1:100,000. The Geological Survey of Israel, Jerusalem
- Eliwa H, Abu El-Enen MM, Khalaf I, Itaya T, Murata M (2008) Metamorphic evolution of Neoproterozoic metapelites and gneisses in the Sinai, Egypt: Insights from petrology, mineral chemistry and K–Ar age dating. *J Afr Earth Sci* 51:107–122. doi:10.1016/j.jafrearsci.2007.12.007
- Eyal Y, Amit O (1984) The Magrish Migmatites (Northeastern Sinai) and their genesis by metamorphic differentiation triggered by a change in the strain orientation. *Isr J Earth Sci* 33:189–200
- Ferrero S, Bartoli O, Cesare B, Salvioli-Mariani E, Acosta-Vigil A, Cavallo A, Groppo C, Battiston S (2012) Microstructures of melt inclusions in anatectic metasedimentary rocks. *J Metamorph Geol* 30:303–322. doi:10.1111/j.1525-1314.2011.00968.x
- Ferry J, Spear F (1978) Experimental calibration of the partitioning of Fe and Mg between biotite and garnet. *Contrib Mineral Petrol* 66:113–117. doi:10.1007/BF00372150
- Fuhrman ML, Lindsley DH (1988) Ternary-feldspar modeling and thermometry. *Am Mineral* 73:201–215
- García-Casco A, Torres-Roldán RL, Millán GPM, Haissen F (2001) High-grade metamorphism and hydrous melting of metapelites in the Pinos terrane (W Cuba): Evidence for crustal thickening and extension in the northern Caribbean collisional belt. *J Metamorph Geol* 19:699–715. doi:10.1046/j.0263-4929.2001.00343.x
- Garfunkel Z (1980) Contribution to the geology of the Precambrian of the Elat area. *Isr J Earth Sci* 29:25–40
- Ghent ED, Stout MZ (1981) Geobarometry and geothermometry of plagioclase–biotite–garnet–muscovite assemblages. *Contrib Mineral Petrol* 76:92–97. doi:10.1007/BF00373688
- Gupta LN, Johannes W (1982) Petrogenesis of a stromatic migmatite (Nelaug, Southern Norway). *J Petrol* 23:548–567. doi:10.1093/petrology/23.4.548
- Gutkin V (1996) Geological mapping of the Mount Shelomo area, Elat. Master’s thesis, Ben-Gurion University of the Negev, Beer Sheva, in Hebrew
- Gutkin V, Eyal Y (1998) Geology and evolution of Precambrian rocks, Mt. Shelomo, Elat area. *Isr J Earth Sci* 47:1–17
- Gutkin V, Vapnik Y, Eyal Y (1999) Fluid-inclusion study and thermometry of migmatites in the Mount Shelomo area (Elat, southern Israel). *Afr Geosci Rev* 6:159–176
- Harris NBW, Caddick M, Kosler J, Goswami S, Vance D, Tindler AG (2004) The pressure–temperature–time path of migmatites from the Sikkim Himalaya. *J Metamorph Geol* 22:249–264. doi:10.1111/j.1525-1314.2004.00511.x

- Hasalová P, Schulmann K, Lexa O, Štípská P, Hrouda F, Ulrich S, Haloda J, Týcová P (2008) Origin of migmatites by deformation-enhanced melt infiltration of orthogneiss: a new model based on quantitative microstructural analysis. *J Metamorph Geol* 26:29–53. doi:[10.1111/j.1525-1314.2007.00743.x](https://doi.org/10.1111/j.1525-1314.2007.00743.x)
- Holland T, Blundy J (1994) Non-ideal interactions in calcic amphiboles and their bearing on amphibole-plagioclase thermometry. *Contrib Mineral Petrol* 116:433–447. doi:[10.1007/BF00310910](https://doi.org/10.1007/BF00310910)
- Holland TJB, Powell R (1998) An internally consistent thermodynamic data set for phases of petrological interest. *J Metamorph Geol* 16:309–343. doi:[10.1111/j.1525-1314.1998.00140.x](https://doi.org/10.1111/j.1525-1314.1998.00140.x)
- Holland TJB, Powell R (2001) Calculation of phase relations involving haplogranitic melts using an internally consistent thermodynamic dataset. *J Petrol* 42:673–683. doi:[10.1093/petrology/42.4.673](https://doi.org/10.1093/petrology/42.4.673)
- Hollister LS, Grissom GC, Peters EK, Stowell HH, Sisson VB (1987) Confirmation of the empirical correlation of Al in hornblende with pressure of solidification of calc-alkaline plutons. *Am Mineral* 72:231–239
- Holness MB, Cesare B, Sawyer EW (2011) Melted rocks under the microscope: Microstructures and their interpretation. *Elements* 7:247–252. doi:[10.2113/gselements.7.4.247](https://doi.org/10.2113/gselements.7.4.247)
- Johannes W (1985) The significance of experimental studies for the formation of migmatites. In: Ashworth, JR (ed) *Migmatites*, Blackie & Son, Glasgow, pp 36–85
- Johannes W, Gupta LN (1982) Origin and evolution of a migmatite. *Contrib Mineral Petrol* 79:114–123. doi:[10.1007/BF01132881](https://doi.org/10.1007/BF01132881)
- Kabesh M, Asran AM, Rahman EA (2012) Mineral chemistry of banded migmatites from Hafafit and Feiran areas, Egypt. *Arab J Geosci*:1–13. doi:[10.1007/s12517-012-0628-0](https://doi.org/10.1007/s12517-012-0628-0)
- Katz O (1997) The metamorphism and the structure of the south eastern Roded block; contribution to the Precambrian basement evolution research. The Hebrew University, Jerusalem, in Hebrew
- Katz O, Avigad D, Matthews A, Heimann A (1998) Precambrian metamorphic evolution of the Arabian–Nubian shield in the Roded area, southern Israel. *Isr J Earth Sci* 47:93–110
- Kleemann U, Reinhardt J (1994) Garnet-biotite thermometry revisited: The effect of Al<sup>VI</sup> and Ti in biotite. *Eur J Mineral* 6:925–941
- Kohn MJ, Spear FS, Valley JW (1997) Dehydration-melting and fluid recycling during metamorphism: Rangeley Formation, New Hampshire, USA. *J Petrol* 38:1255–1277. doi:[10.1093/ptro/38.9.1255](https://doi.org/10.1093/ptro/38.9.1255)
- Kretz R (1983) Symbols for rock-forming minerals. *Am Mineral* 68:277–279
- Mahar EM, Baker JM, Powell R, Holland TJB, Howell N (1997) The effect of Mn on mineral stability in metapelites. *J Metamorph Geol* 15:223–238. doi:[10.1111/j.1525-1314.1997.00011.x](https://doi.org/10.1111/j.1525-1314.1997.00011.x)
- Matthews A, Reymer APS, Avigad D, Cochín J, Marco S (1989) Pressures and temperatures of Pan-African high-grade metamorphism in the Elat Association, NE Sinai. *Isr J Earth Sci* 38:1–17
- Morag N, Avigad D, Gerdes A, Belousova E, Harlavan Y (2011) Crustal evolution and recycling in the northern Arabian–Nubian Shield: New perspectives from zircon Lu–Hf and U–Pb systematics. *Precambrian Res* 186:101–116. doi:[10.1016/j.precamres.2011.01.004](https://doi.org/10.1016/j.precamres.2011.01.004)
- Nabelek PI, Bartlett CD (1998) Petrologic and geochemical links between the post-collisional Proterozoic Harney Peak leucogranite, South Dakota, USA, and its source rocks. *Lithos* 45:71–85. doi:[10.1016/S0024-4937\(98\)00026-7](https://doi.org/10.1016/S0024-4937(98)00026-7)
- Passchier CW, Trouw RAJ (2005) *Microtectonics*, 2nd edn. Springer-Verlag, Berlin, Germany
- Patiño Douce AE, Harris N (1998) Experimental constraints on Himalayan anatexis. *J Petrol* 39:689–710. doi:[10.1093/ptro/39.4.689](https://doi.org/10.1093/ptro/39.4.689)
- Perchuk LL, Lavrent'eva IV (1983) Experimental investigation of exchange equilibria in the system cordierite-garnet-biotite. In: Saxena SK (ed) *Kinetics and equilibrium in mineral reactions, advances in physical geochemistry*, vol 3, pp 199–239
- Peterman EM, Grove M (2010) Growth conditions of symplectic muscovite + quartz: Implications for quantifying retrograde metamorphism in exhumed magmatic arcs. *Geology* 38:1071–1074. doi:[10.1130/G31449.1](https://doi.org/10.1130/G31449.1)
- Petrík I, Janák M (2002) Migmatites and leucogranites produced by muscovite dehydration melting on the example of the Strážovské Vrchy Mts. (Suchý Core), Western Carpathians. *Geolines* 14:74–75
- Pognante U (1992) Migmatites and leucogranites of tertiary age from the high Himalayan Crystallines of Zaskar (NW India): a case history of anatexis of Palaeozoic orthogneisses. *Mineral Petrol* 46:291–313. doi:[10.1007/BF01173569](https://doi.org/10.1007/BF01173569)
- Ragab AI, El-Gharabawi RI (1989) Wadi El-Hudi migmatites, east of Aswan, Egypt: a geological study and some geotectonic implications for the eastern desert of Egypt. *Precambrian Res* 44:67–79. doi:[10.1016/0301-9268\(89\)90076-4](https://doi.org/10.1016/0301-9268(89)90076-4)
- Sadek Ghabrial D (2003) Petrological study of Taba migmatites, east central Sinai, Egypt. *MERC Ain Shams Univ. Earth Sci Ser* 17:58–72
- Sawyer EW (1987) The role of partial melting and fractional crystallization in determining discordant migmatite leucosome compositions. *J Petrol* 28:445–473. doi:[10.1093/petrology/28.3.445](https://doi.org/10.1093/petrology/28.3.445)
- Sawyer EW (1999) Criteria for the recognition of partial melting. *Phys Chem Earth Pt A* 24:269–279. doi:[10.1016/S1464-1895\(99\)00029-0](https://doi.org/10.1016/S1464-1895(99)00029-0)
- Sawyer EW (2008a) *Atlas of Migmatites*. The Canadian Mineralogist. Special Publication 9, NRC Research Press, Ottawa
- Sawyer EW (2008b) Working with migmatites; nomenclature for the constituent parts. In: Sawyer EW, Brown M (eds) *Working with migmatites, Short Course Series - Mineralogical Association of Canada*, vol 38. Mineralogical Association of Canada, Quebec, pp 1–28
- Sawyer EW, Cesare B, Brown M (2011) When the continental crust melts. *Elements* 7:229–234. doi:[10.2113/gselements.7.4.229](https://doi.org/10.2113/gselements.7.4.229)
- Shimron AE (1972) The Precambrian structural and metamorphic history of the Elat area. PhD thesis. The Hebrew University, Jerusalem
- Solar GS (2008) The interplay between tectonics/structure and migmatite morphology in the field. In: Sawyer EW, Brown M (eds) *Working with migmatites, Short Course Series - Mineralogical Association of Canada*, vol 38. Mineralogical Association of Canada, Quebec, pp 145–158
- Solar GS, Brown M (2001) Petrogenesis of migmatites in Maine, USA: Possible source of peraluminous leucogranite in plutons? *J Petrol* 42:789–823. doi:[10.1093/petrology/42.4.789](https://doi.org/10.1093/petrology/42.4.789)
- Spear FS, Kohn MJ, Cheney JT (1999) *P–T* paths from anatectic pelites. *Contrib Mineral Petrol* 134:17–32. doi:[10.1007/s004100050466](https://doi.org/10.1007/s004100050466)
- Stern RJ (1994) Arc assembly and continental collision in the Neoproterozoic East African Orogen: Implications for the consolidation of Gondwanaland. *Annu Rev Earth Planet Sci* 22:319–351. doi:[10.1146/annurev.earth.22.050194.001535](https://doi.org/10.1146/annurev.earth.22.050194.001535)
- Tajčmanová L, Connolly JAD, Cesare B (2009) A thermodynamic model for titanium and ferric iron solution in biotite. *J Metamorph Geol*:153–165. doi:[10.1111/j.1525-1314.2009.00812.x](https://doi.org/10.1111/j.1525-1314.2009.00812.x)
- Thompson AB (1982) Dehydration melting of pelitic rocks and the generation of H<sub>2</sub>O-undersaturated granitic liquids. *Am J Sci* 282:1567–1595. doi:[10.2475/ajs.282.10.1567](https://doi.org/10.2475/ajs.282.10.1567)

- Väisänen M, Hölttä P (1999) Structural and metamorphic evolution of the Turku migmatite complex, southwestern Finland. *Bull Geol Soc Finl* 71:177–218
- Vernon RH (2004) *A Practical Guide to Rock Microstructure*. Cambridge University Press, Cambridge. doi:[10.2277/0521891337](https://doi.org/10.2277/0521891337)
- Vernon RH (2011) Microstructures of melt-bearing regional metamorphic rocks. In: van Reenen DD, Kramers JD, McCourt S, Perchuk L (eds) *Origin and evolution of precambrian high-grade gneiss terranes, with special emphasis on the Limpopo complex of Southern Africa*. *Geol Soc Am Mem*, vol 207, pp 1–11. doi:[10.1130/2011.1207\(01\)](https://doi.org/10.1130/2011.1207(01))
- Vernon RH, Collins WJ (1988) Igneous microstructures in migmatites. *Geology* 16:1126–1129. doi:[10.1130/0091-7613\(1988\)016<1126:IMIM>2.3.CO;2](https://doi.org/10.1130/0091-7613(1988)016<1126:IMIM>2.3.CO;2)
- White AJR (1966) Genesis of migmatites from the Palmer region of south Australia. *Chem Geol* 1:165–200. doi:[10.1016/0009-2541\(66\)90015-5](https://doi.org/10.1016/0009-2541(66)90015-5)
- White RW, Powell R, Holland TJB (2001) Calculation of partial melting equilibria in the system Na<sub>2</sub>O–CaO–K<sub>2</sub>O–FeO–MgO–Al<sub>2</sub>O<sub>3</sub>–SiO<sub>2</sub>–H<sub>2</sub>O (NCKFMASH). *J Metamorph Geol* 19:139–153. doi:[10.1046/j.0263-4929.2000.00303.x](https://doi.org/10.1046/j.0263-4929.2000.00303.x)
- Whitney DL, Irving AJ (1994) Origin of K-poor leucosomes in a metasedimentary migmatite complex by ultrametamorphism, syn-metamorphic magmatism and subsolidus processes. *Lithos* 32:173–192. doi:[10.1016/0024-4937\(94\)90038-8](https://doi.org/10.1016/0024-4937(94)90038-8)
- Yuguchi T, Nishiyama T (2008) The mechanism of myrmekite formation deduced from steady-diffusion modeling based on petrography: Case study of the Okueyama granitic body, Kyushu, Japan. *Lithos* 106:237–260. doi:[10.1016/j.lithos.2008.07.017](https://doi.org/10.1016/j.lithos.2008.07.017)